ISSN 0030-400X, Optics and Spectroscopy, 2021, Vol. 129, No. 3, pp. 363–368. © Pleiades Publishing, Ltd., 2021.
ISSN 0030-400X, Optics and Spectroscopy, 2021. © Pleiades Publishing, Ltd., 2021.
Russian Text © The Author(s), 2021, published in Optika i Spektroskopiya, 2021, Vol. 129, No. 3, pp. 266–271.

Emission Spectra of Heavy Inert Gases Kr and Xe in the Range from 3 to 20 nm Obtained under Pulsed Laser Excitation Using Various Gas Jets as Targets

A. N. Nechai[a], *, A. A. Perekalov[a], N. N. Salashchenko[a], and N. I. Chkhalo[a]

[a] *Institute for Physics of Microstructures, Russian Academy of Sciences, Nizhny Novgorod, 603087 Russia*

**e-mail: nechay@ipm.sci-nnov.ru*

Received November 19, 2020; revised November 19, 2020; accepted November 30, 2020

Abstract—Results of investigation of emission spectra of Kr and Xe under pulsed laser excitation are presented. Spectral range between 3 and 20 nm was studied using a Nd:YAG laser (λ = 1064 nm, τ = 5 ns, E_{pulse} = 0.8 J). A capillary tube with d = 500 μm, along with supersonic conical nozzles with d_{cr} = 145 μm, $2\alpha = 12°$, L = 5 mm and d_{cr} = 540 μm, $2\alpha = 11°$, L = 5 mm were used for gas-jet formation. Emission spectra were obtained for various gas targets, interpreted, and ions emitting in the spectral range under consideration were identified. Intensities of lines obtained with targets formed by different systems are compared.

Keywords: cluster beams, extreme ultraviolet (EUV) radiation, emission spectra, laser spark, X-ray spectrometer–monochromator

DOI: 10.1134/S0030400X21030127

INTRODUCTION

Studies in spectral regions of short-wavelength radiation, soft X-ray (SXR) and extreme ultraviolet (EUV), in particular, are currently a hot topic of research. Earlier studies in the SXR and EUV spectral ranges with application of multi-layer optics were related to diagnostics of laboratory and space plasma [1], along with solution of problems of short-wavelength projection lithography [2]. Currently, laboratory applications using SXR and EUV technology become dominant. In particular, these are studies related to investigation of structure and ordering of nanosized objects, both natural and man-made [3].

Plasma sources, including those in which plasma is created by means of pulsed laser radiation (PLR sources), are used for laboratory purposes most frequently [4–6]. Gas jets [4, 7], solid [8, 9], and frozen gas targets [10, 11] are used as targets for pulsed excitation.

We studied emission properties of light inert gases using various systems of gas-target formation earlier. In the present work, we continue these studies and investigate emission properties of heavy inert gases.

EXPERIMENTAL SETUP

The experimental setup described in detail in [12] was used in the present study. The setup operated as follows. The gas being studied was fed into a conical supersonic nozzle, creating a gas target upon outflow into a vacuum chamber. The chamber was pumped out by means of cryogenic condensation and absorption pumps. Laser radiation was incident on a short-focal-distance lens that induced laser breakdown and plasma formation in its focus. Polychromic SXR and EUV plasma radiation propagated through a free-hanging X-ray filter and was incident on the input mirror of RSM-500 spectrometer–monochromator. Monochromatic SXR and EUV radiation was detected by a pulsed detector.

An NL300 Series Nd:YAG laser with the following parameters: wavelength of 1064 nm, pulse energy of 0.8 J, pulse width of 5.2 ns, and pulse repetition rate of up to 10 Hz was used for excitation of an atomic-cluster jet. Laser radiation was focused into the gas target by means of a lens with a focal distance of 45 mm. Calculated focal-spot diameter was 66 μm. A free-hanging $Mo/ZrSi_2$ filter with bi-layer thicknesses of 1.5/2.5 nm and the number of layers equal to 12 was used. The free-hanging filter served also for protection from particles of different nature formed in the process of SXR/EUV source operation.

Spectral resolution of the device measured at the L-edges of absorption of the silicon and aluminum free-hanging filters and at the K-edge of the beryllium one, as well as from the half-width of the zero order, was found to be 0.04 nm. The studied wavelength range for the grating and mirror used in the study was 3–20 nm.

The following nozzles were used for forming gas-jet targets: a small supersonic conical nozzle with d_{cr} = 145 μm, 2α = 12°, L = 5 mm; a large supersonic conical nozzle with d_{cr} = 540 μm, 2α = 11°, L = 5 mm; a capillary tube with d = 500 μm. These systems of gas-jet formation had specific features described below.

A conical supersonic nozzle of small critical cross section (d_{cr} = 145 μm) formed a directed supersonic gas jet. Upon feeding cooled gas or gas at high pressure into the nozzle, a cluster beam containing a large portion of condensate and exhibiting a narrow directional pattern was formed. These nozzles can be used at different gas temperatures and pressures in the presence of evacuating systems of acceptable capacity (~1000 L/s). As a rule, such nozzles are used for forming cluster beams under the regime of constant gas outflow and are convenient when laser systems with high pulse repetition rate are used.

A conical supersonic nozzle of large critical cross section (d_{cr} = 540 μm) also formed a directed supersonic gas jet. However, large critical cross section leads to high gas consumption, which requires using a pulsed valve when using evacuating systems of acceptable capacity (~1000 L/s). Using fast pulsed valves, in turn, limits the range of gas pressures that can be used and gas temperature at the nozzle input, in particular, which does not allow obtaining cluster beams characterized by large cluster size. Application of pulsed valves requires using laser systems with a low (~10 Hz) pulse repetition rate.

A capillary tube of large cross section d = 500 μm is characterized by the sonic regime of gas outflow that forms a cloud upon nearly isotropic expansion in all directions from the edge of the capillary tube. Large tube diameter leads to high gas consumption, which also requires using a pulsed valve when using evacuating systems of acceptable capacity (~1000 L/s). At the same time, this system of gas-jet target formation is the simplest and most reliable one.

In general, gas jets formed in the process of gas outflow from conical nozzles into vacuum have complex spatial structure determined by gas parameters at the nozzle input and geometrical parameters of the nozzle itself. Problems related to description of atomic-cluster jets formed as a result of ejection of condensing gas from supersonic nozzles into vacuum are particularly complex. Gas-dynamic calculation of structure of such an atomic-cluster target is very labor intensive and represents a separate problem. Based on the results obtained in [4], we assumed in our study that particle concentration in the gas jets was ~10^{19} particles/cm^3.

RESULTS

Investigation of Krypton Gas-Jet Targets

Krypton is a heavy inert gas, which automatically makes it a relatively convenient target for creation of a laser-plasma source of SXR and EUV radiation that demonstrates high radiation intensity with a large number of bright lines. Krypton as a target was studied in [7, 13–15], where, unfortunately, observed emission lines were not identified and their relative intensity was not indicated.

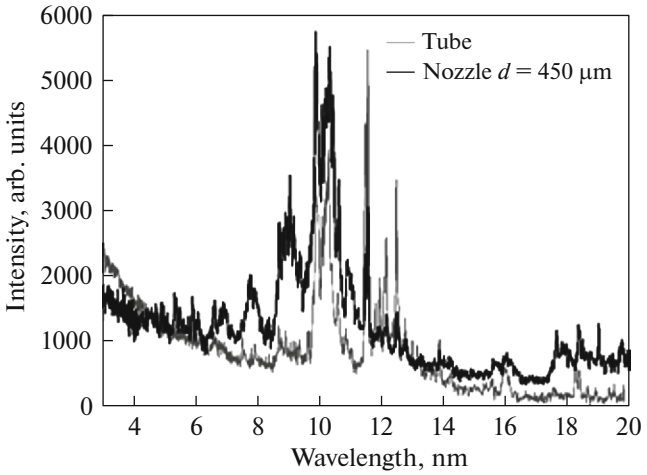

Fig. 1. Emission spectra of krypton targets obtained using a capillary tube and a conical nozzle with d_{cr} = 540 μm as jet sources.

An emission spectrum of krypton obtained using a capillary tube and a conical nozzle with a critical cross section of 450 μm for gas pressure at the nozzle input equal to 3 bar and gas temperature of 300 K is presented in Fig. 1. The wavelength range between 3 and 20 nm was studied. Intensity is shown in arbitrary units.

A number of intense lines in the range from 6 and 20 nm that are associated with transitions in Kr-VIII, Kr-IX, and Kr-X ions can be seen. Emission lines between 9 and 11 nm merge together to form spectral bands. It can be seen that using a supersonic nozzle with d_{cr} = 540 μm results in considerable redistribution of intensities of krypton emission lines, accompanied by growth of intensities of the lines corresponding to Kr-X. Identification of observed lines was carried out according to [16–18] and is presented in Table 1.

Relative intensities of the lines for spectra obtained using different systems of target formation are presented in Table 2. Particle concentration in the laser-spark region increases in the following order: capillary tube, 145-μm nozzle (3 bar), 145-μm nozzle (6 bar), 450-μm nozzle (3 bar).

The following conclusions can be made based on the data presented in Table 2.

Upon increase in particle concentration in the discharge region, relative intensity of lines corresponding to Kr-X ions in high charge states increases, which corresponds to growth of plasma temperature. Relatively large change in intensity, up to fivefold, is

Table 1. Emission lines of krypton

Wavelength, nm	Intensity, arb. units	Ion	Transition
6.61	600	Kr-IX	$3d^{10}-3d^{9}5f$
7.54	500	Kr-IX	$3d^{10}-3d^{9}4f$
7.62	550	Kr-IX	$3d^{10}-3d^{9}4f$
7.68	300	Kr-IX	$3d^{10}-3d^{9}4f$
9.18	500	Kr-X	$3p^{6}3d^{9}-3p^{6}3d^{8}4p$
9.66	650	Kr-X	$3p^{6}3d^{9}-3p^{5}3d^{10}$
9.84	1300	Kr-X	$3p^{6}3d^{9}-3p^{6}3d^{8}4p$
9.9	3300	Kr-X	$3p^{6}3d^{9}-3p^{6}3d^{8}4p$
10.02	2450	Kr-X	$3p^{6}3d^{9}-3p^{6}3d^{8}4p$
10.14	2700	Kr-X	$3p^{6}3d^{9}-3p^{6}3d^{8}4p$
10.26	2900	Kr-X	$3p^{6}3d^{9}-3p^{6}3d^{8}4p$
10.32	3450	Kr-X	$3p^{6}3d^{9}-3p^{6}3d^{8}4p$
10.35	1650	Kr-X	$3p^{6}3d^{9}-3p^{6}3d^{8}4p$
10.4	1250	Kr-X	$3p^{6}3d^{9}-3p^{6}3d^{8}4p$
11.49	3900	Kr-IX	$3d^{10}-3d^{9}4p$
11.57	5000	Kr-IX	$3d^{10}-3d^{9}4p$
11.77	1100	Kr-IX	$3d^{10}-3d^{9}4p$
11.82	1500	Kr-VIII	$4s-3d^{9}4s4p$
11.94	1500	Kr-VIII	$4s-3d^{9}4s4p$
12.15	2100	Kr-VIII	$4p-3d^{9}4p^{2}$
12.38	800	Kr-VIII	$4s-3d^{9}4s4p$
12.47	3000	Kr-VIII	$4s-3d^{9}4s4p$
12.77	800	Kr-VIII	$4s-3d^{9}4s4p$
13.84	1000	Kr-VIII	$4s-6p$
14.21	550	Kr-VIII	$4p-8s$
15.31	350	Kr-VIII	$4p-7s$
15.55	400	Kr-VIII	$4p-7s$
16.0	600	Kr-VIII	$4p-6d$
18.16	800	Kr-VIII	$4s-5p$
18.29	550	Kr-VIII	$4s-5p$
18.55	300	Kr-VIII	$4p-6s$
19.46	350	Kr-VIII	$4p-3d^{9}4s^{2}$
19.85	350	Kr-VIII	$4p-3d^{9}4s^{2}$

observed. At the same time, observed change in plasma temperature does not result in appearance of emission lines corresponding to krypton ions in other charge states.

Relative intensity of emission lines for ions in the same charge state obtained using different gas targets varies. These changes are relatively large, reaching 50% in our experiments.

In general, the results of studies of krypton emission spectra allow making several conclusions listed below.

Ionization energy for Kr-X ion equals 275 eV, while that of the next ion (Kr-XI) emission lines of which were not observed in the discussed experiment equals 316 eV.

It can be seen from the experimental data that the shape of the krypton emission spectrum does not change qualitatively for the studied types of targets. Consequently, is can be stated that lines that belong to ions in the same charge state will appear in emission spectra for any gas target similar to the one studied. The spectra can differ only with respect to intensity of observed emission lines. Intensity of the obtained emission lines can be substantially altered by changing parameters of gas outflow from the nozzle.

The number of particles in the laser-spark region must be increased substantially in order to induce a qualitative change in the shape of spectra and obtain ions in a higher charge state.

Investigation of Xenon Gas-Jet Targets

Investigation of xenon as a target of a laser-plasma source of radiation in the SXR and EUV spectral ranges was carried out in a large number of studies (see, e.g., [13, 14, 19, 20]). As a rule, main attention in these studied was paid to unresolved transition arrays (UTA) in the region of ~10.5 nm. At the same time, other emission bands are of interest for laboratory applications, too [6, 7].

Emission spectrum of xenon obtained using a capillary tube and a conical nozzle with a critical cross section of 450 μm at gas pressure at the nozzle input equal to 3 bar and gas temperature of 300 K is presented in Fig. 2. The spectral interval from 5 to 20 nm was studied. Radiation intensity is plotted in arbitrary units.

A number of intense lines associated with transitions in Xe-VIII, Xe-IX, and Xe-X ions can be seen in the interval between 8 and 18 nm. A UTA band (10–12 nm) studied in a large number of works (see, e.g., [21, 22]) dominates the spectrum. It can be seen that using a supersonic nozzle leads to substantial change in the UTA band related to changes in radiation absorption in the gas jet and residual gas (Xe) contained in the chamber [23]. Recorded spectra of xenon in the range between 10 and 15 nm strongly depend of radiation absorption in the gas jet and residual gas (Xe), which gives rise to an extremely strong dependence on the jet-target structure. The gas target has to be designed individually for each experimental setup in order to obtain optimal operating parameters of the

Table 2. Relative intensities of the lines of krypton obtained using different systems of target formation

Wavelength, nm	Ion	Intensities for different targets, arb. units			
		capillary tube, 3 bar	nozzle 450 μm, 3 bar	nozzle 145 μm, 3 bar	nozzle 145 μm, 6 bar
9.9	Kr-X	1	1	1	1
10.14	Kr-X	0.76	0.75	0.84	0.83
10.32	Kr-X	1.11	0.98	0.92	0.99
10.4	Kr-X	0.39	0.51	0.60	0.60
11.49	Kr-IX	1.26	0.29	0.45	0.31
11.57	Kr-IX	1.64	0.47	0.71	0.52
12.15	Kr-VIII	0.68	0.13	0.15	0.10
12.47	Kr-VIII	0.99	0.15	0.23	0.17

SXR/EUV source. This kind of research has to be mainly experimental, because simulation of supersonic jets with gas condensation represents a rather complex problem.

The observed spectral lines were identified according to [16, 17, 24] and are listed in Table 3.

Relative intensities of the lines obtained using different systems of target formation are presented in Table 4.

The data presented in Table 4 allow making several conclusions listed below.

Relative intensities of the lines corresponding to ions in high change states (Xe-XI) increase with increase in particle concentration in the discharge region, which corresponds to rise in plasma temperature. Intensity changes considerably, up to sevenfold. At the same time, observed changes in plasma temperature do not cause an appearance of Xe ions in other charge states.

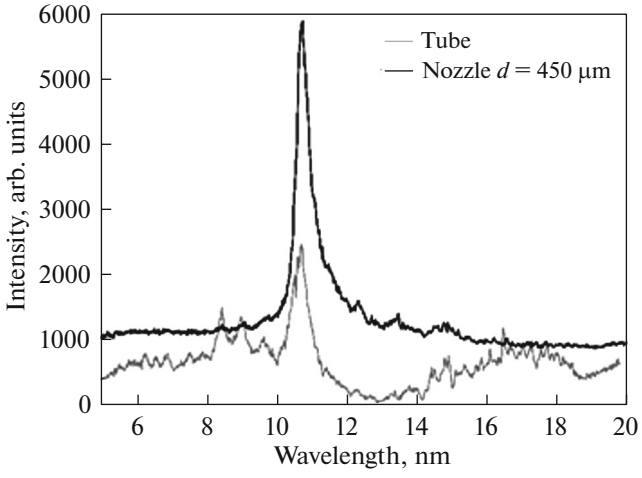

Fig. 2. Emission spectra of xenon targets obtained using a capillary tube and a conical nozzle with d_{cr} = 540 μm as jet sources.

Relative intensity of emission lines for ions in the same charge state varies depending on the gas target used. These changes are relatively large, reaching 150% in our experiments.

In general, several conclusions listed below can be made as a result of investigation of emission spectra of xenon.

Ionization energy for Xe-XI ion equals 229 eV, while that for Xe-XII ion the emission lines of which were not observed in the discussed experiment equals 264 eV.

It can be seen from the experimental data that the shape of the obtained spectrum of xenon qualitatively changes depending on the type of target used. Variation in particle concentration in the spark region was achieved by changing the jet-target structure, which results in strong changes in distribution of xenon particles in the chamber volume. This, in turn, changes absorption of SRX and EUV radiation by residual xenon, which dramatically modifies obtained spectra. This situation results in obtained spectra being specific for each gas-jet source and each regime of gas outflow.

Note that using supersonic gas jets offers some advantages. In the discussed case, the gas jet propagates within a narrower solid angle and exhibits higher density when the chamber contains less scattered gas.

CONCLUSIONS

In the present study, we obtained emission spectra of a laser-plasma source with gas-jet targets formed by heavy inert gases (Kr, Xe) in the wavelength range between 3 and 20 nm. The targets were formed by means of various nozzles at different values of gas pressure at the nozzle input.

1. Emission spectra of a laser-plasma source using various gas targets formed by heavy inert gases (krypton and xenon) were obtained. The spectra were inter-

Table 3. Emission lines of xenon

Wavelength, nm	Intensity, arb. units	Ion	Transition
8.54	3750	Xe-IX	$4d^{10}–4d^{9}6f$
8.84	3700	Xe-IX	$4d^{10}–4d^{9}7p$
9.64	3300	Xe-IX	$4d^{10}–4d^{9}5f$
10.65	7000	UTA	UTA
11.34	2600	Xe-IX	$4d^{9}–4d^{8}4f$
12.01	2000	Xe-IX	$4d^{10}–4d^{9}4f$
12.64	1800	Xe-XI	$4d^{8}–4d^{7}4f$
13.23	1850	Xe-XI	$4d^{8}–4d^{7}5p$
13.8	1850	Xe-XI	$4d^{8}–4d^{7}5p$
14.2	1750	Xe-X	$4d^{9}–4d^{8}5p$
14.36	2150	Xe-IX	$4d^{10}–4d^{9}4f$
14.47	2250	Xe-X	$4d^{9}–4d^{8}5p$
14.77	2450	Xe-X	$4d^{9}–4d^{9}4f$
14.86	2400	Xe-X	$4d^{9}–4d^{8}5p$
15.06	2150	Xe-X	$4d^{9}–4d^{8}5p$
15.28	2125	Xe-X	$4d^{9}–4d^{8}5p$
15.63	2050	Xe-X	$4d^{9}–4d^{8}5p$
15.89	2150	Xe-X	$4d^{9}–4p^{5}4d^{10}$
16.17	2500	Xe-IX	$4d^{10}–4d^{9}5p$
16.5	3000	Xe-IX	$4d^{10}–4d^{9}5p$
16.67	2300	Xe-VIII	$5s–4d^{9}5s5p$
17.09	2500	Xe-VIII	$5s–4d^{9}5s5p$
17.4	2450	Xe-VIII	$5s–4d^{9}5s5p$
17.58	2400	Xe-VIII	$5s–4d^{9}5s5p$
17.72	2450	Xe-VIII	$5s–4d^{9}5s5p$
17.97	2300	Xe-VIII	$5s–4d^{9}5s5p$
18.17	2100	Xe-VIII	$5s–4d^{9}5s5p$

preted, and ions emitting in the discussed spectral range were identified.

For krypton, spectra of gas targets of various structure did not experience substantial charges upon changing gas pressure at the nozzle input. For xenon, the obtained spectra were individual and were determined by several factors, such as jet structure, scattered gas flows, and experimental-setup geometry.

The highest ion charge states achieved in our experiments were Kr-X and Xe-XI.

2. Changes in emission spectra obtained with various nozzles forming gas jets of different structure at different values of gas pressure at the nozzle input were determined.

Table 4. Relative intensities of the lines of xenon obtained using different systems of target formation

Wavelength, nm	Ion	Intensity for different targets, arb. μnits	
		capillary tube, 3 bar	nozzle 450 μm, 3 bar
8.54	Xe-IX	0.44	0.03
8.84	Xe-IX	0.41	0.04
9.64	Xe-IX	0.30	0.07
10.65	UTA	1.00	1.00
11.34	Xe-IX	0.17	0.24
12.01	Xe-IX	0.10	0.12
13.23	Xe-XI	0.08	0.08
14.77	Xe-X	0.27	0.06
14.86	Xe-X	0.28	0.06
16.17	Xe-IX	0.30	0.02
16.5	Xe-IX	0.42	0.02

It was found that intensity of emission lines corresponding to ions in high charge states increases and, correspondingly, plasma temperature rises with increase in particle concentration at the nozzle input. Also, intensities of lines for emitting ions in the same charge state redistribute upon increase in gas concentration in the discharge region. This phenomenon is completely determined by an increase in concentration of gas particles in the laser-spark region when using different systems of gas-jet formation. At the same time, the highest charge number of ions remains the same.

Intensities of individual emission lines can thus be varied in a wide range by using gas targets of different structure and varying pressure at their input. A sharp increase in the number of particles in the discharge region is required in order to induce qualitative changes in the spectra, which can be achieved either by increasing pressure at the nozzle input or by increasing the critical cross section of the nozzle. Using nozzles of small cross section in combination with high gas pressure at the nozzle input creates optimal conditions for increasing plasma temperature and radiation intensity while minimizing the requirements to the evacuation system [25]. A similar result can be achieved by using liquid targets [26].

FUNDING

This research was supported by the Russian Foundation for Basic Research, projects nos. 19-02-00081, 19-07-00173, 20-02-00708, and 20-02-00364.

CONFLICT OF INTEREST

The authors declare that they have no conflict of interest.

REFERENCES

1. S. V. Kuzin, V. N. Polkovnikov, and N. N. Salashchenko, Bull. Russ. Acad. Sci.: Phys. **75**, 84 (2011).
2. N. I. Chkhalo and N. N. Salashchenko, AIP Adv. **3**, 082130 (2013).
3. W. Chao, B. D. Harteneck, J. A. Liddle, E. H. Anderson, and D. T. Attwood, Nature (London, U.K.) **435** (7046), 1210 (2005).
4. M. Suzuki, H. Daido, I. W. Choi, W. Yu, K. Nagai, T. Norimatsu, and H. Fiedorowicz, Phys. Plasma **10**, 227 (2003).
5. M. B. Smirnov and W. Becker, Phys. Rev. A **74**, 013201 (2006).
6. N. I. Chkhalo, S. A. Garakhin, S. V. Golubev, A. Ya. Lopatin, A. N. Nechay, A. E. Pestov, N. N. Salashchenko, M. N. Toropov, N. N. Tsybin, A. V. Vodopyanov, and S. Yulin, Appl. Phys. Lett. **112**, 221101 (2018).
7. H. Fiedorowicz, A. Bartnik, M. Szczurek, H. Daido, N. Sakaya, V. Kmetik, and T. Nakayama, Opt. Commun. **163**, 103 (1999).
8. Y. Tao, M. S. Tillack, K. L. Sequoia, R. A. Burdt, S. Yuspeh, and F. Najmabadi, Appl. Phys. Lett. **92**, 251501 (2008).
9. T. Higashiguchi, T. Otsuka, N. Yugami, W. Jiang, A. Endo, B. Li, D. Kilbane, P. Dunne, and G. O'Sullivan, Appl. Phys. Lett. **99**, 191502 (2011).
10. K. Fukugaki, S. Amano, A. Shimoura, T. Inoue, S. Miyamoto, and T. Mochizuki, Rev. Sci. Instrum. **77**, 063114 (2006).
11. B. A. M. Hansson, O. Hemberg, and H. M. Hertz, Rev. Sci. Instrum. **75**, 2122 (2004).
12. A. N. Nechay, N. N. Salashchenko, and N. I. Chkhalo, J. Surf. Invest.: X-ray, Synchrotron Neutron Tech. **11**, 496 (2017).
13. A. Bartnik, H. Fiedorowicz, P. Wachulak, and T. Fok, Laser Part. Beams **36**, 286 (2018).
14. S. Kranzusch and K. Mann, Opt. Commun. **200**, 223 (2001).
15. A. N. Nechai, S. A. Garakhin, A. Ya. Lopatin, V. N. Polkovnikov, D. G. Reunov, N. N. Salashchenko, M. N. Toropov, N. I. Chkhalo, and N. N. Tsybin, Quantum Electron. **50**, 408 (2020).
16. *NIST Atomic Spectra Database* (Gaithersburg, 2009–2019). www.nist.gov/pml/atomic-spectra-database.
17. R. L. Kelly and L. J. Palumbo, Report No. NRL-7599 (Naval Res. Lab., Washington DC, 1973).
18. E. B. Saloman, J. Phys. Chem. Ref. Data **36**, 215 (2007).
19. G. Kooijman, Thesis (FOM Inst., 2003).
20. N. I. Chkhalo, S. A. Garakhin, A. Ya. Lopatin, A. N. Nechay, A. E. Pestov, V. N. Polkovnikov, N. N. Salashchenko, N. N. Tsybin, and S. Yu. Zuev, AIR Adv. **8**, 105003 (2018).
21. F. Gilleron, M. Poirier, T. Blenski, M. Schmidt, and T. Ceccotti, J. Appl. Phys. **94**, 2086 (2003).
22. V. P. Belik, S. G. Kalmykov, A. M. Mozharov, M. V. Petrenko, and M. E. Sasin, Tech. Phys. Lett. **43**, 1001 (2017).
23. R. de Bruijn, K. Koshelev, G. Kooijman, E. S. Toma, and F. Bijkerk, J. Quant. Spectrosc. Radiat. Transfer **81**, 97 (2003).
24. E. B. Saloman, J. Phys. Chem. Ref. Data **33**, 765 (2004).
25. M. Müller, T. Mey, J. Niemeyer, M. Lorenz, and K. Mann, AIP Conf. Proc. **1764**, 030003 (2016).
26. B. A. M. Hansson and H. M. Hertz, J. Phys. D: Appl. Phys. **37**, 3233 (2004).